applied sciences

MDPI

Article

Analysis and Prediction of Mid-High Peak Frequency for Microspeaker with Side-Firing Front Chamber †

Zhi-Xiong Jiang [1], Ji-Hun Park [1], Dan-Ping Xu [2] and Sang-Moon Hwang [1,*]

[1] School of Mechanical Engineering, Pusan National University, Busan 46241, Republic of Korea
[2] School of Mechatronic Engineering and Automation, Shanghai University, Shanghai 200444, China
* Correspondence: shwang@pusan.ac.kr; Tel.: +82-051-510-3204
† This paper is an extension of work originally presented in the conference on electromagnetic field computation (CEFC), 24 October 2022.

Featured Application: Audio module of smartphone or other multimedia devices.

Abstract: The generating mechanisms of the mid-high-frequency peaks of a sound pressure level are theoretically investigated in this study with a side-firing front chamber. A mid-frequency peak is caused by the Helmholtz resonance phenomenon of the front chamber, and a high-frequency peak occurs owing to tube resonance. The electromagnetic–mechanical–acoustic coupling method (E–M–A) and resonance equations are used to obtain the sound pressure level and peak frequencies, respectively. Seven side-firing front chambers have been designed with respect to different tube lengths, tube widths and tube heights. Microspeaker samples with different front chamber designs are manufactured to verify the analytical results. The SPL and mid-high peak frequencies comparisons showed good agreement between the analysis and experimental results.

Keywords: acoustic tube; Helmholtz resonator; microspeaker; sound pressure level

check for updates

Citation: Jiang, Z.-X.; Park, J.-H.; Xu, D.-P.; Hwang, S.-M. Analysis and Prediction of Mid-High Peak Frequency for Microspeaker with Side-Firing Front Chamber. *Appl. Sci.* **2023**, *13*, 1018. https://doi.org/10.3390/app13021018

Academic Editor: Dimitrios G. Aggelis

Received: 8 December 2022
Revised: 9 January 2023
Accepted: 10 January 2023
Published: 11 January 2023

Copyright: © 2023 by the authors. Licensee MDPI, Basel, Switzerland. This article is an open access article distributed under the terms and conditions of the Creative Commons Attribution (CC BY) license (https://creativecommons.org/licenses/by/4.0/).

1. Introduction

Nowadays, portable devices such as smartphones, tablet PCs and smartwatches are frequently used in our daily lives. These devices are capable of performing many tasks such as making phone calls, internet browsing, playing music, etc. An increasing number of people use smartphones to consume entertaining content and the demand for multimedia content keep increasing. Among many factors, sound plays a vital role for users enjoying multimedia content. Thus, the acoustic performance of a smartphone is an important consideration of consumers when they select smartphones. Microspeakers, as electroacoustic transducers, are responsible for generating sound and providing alarming feedback in multimedia devices. There are several types of electroacoustic transducers that have been developed in recent years; they have different working principles. This is an extended and revised version of a preliminary conference report that was presented at a conference on electromagnetic field computation (CEFC) 2022 [1].

In the earlier era of cellular phones, a round microspeaker was used. A round and elliptical shape microspeaker was introduced and analyzed by Hwang et al. An elliptical and a circular microspeaker both resulted in an equivalent performance [2]. Adding a permanent magnet at the center, the SPL was increased [3]. Owing to the high demand for mobile phones with a large display and a small microspeaker that can utilize space more efficiently, a rectangular microspeaker was developed by Kwon et al. In addition, a new magnetic circuit was analyzed using the three-dimensional finite element method (3D FEM) to reduce the width size [4]. For a slimmer microspeaker with good acoustic performance, Lee et al. analyzed a novel magnetic circuit that excluded the top plate and placed horizontally magnetized permanent magnets [5].

The balanced armature receiver [6,7] is one of most popular electroacoustic transducers to provide a good acoustic performance, and it has been widely used in hearing aids and earphones because of its small size. The working principle of balanced armature is that, when electric current is passed through the voice, the flux density on the upper surface of the armature is bigger than on the lower surface of the armature. Then, the electromagnetic force is generated on the armature to contribute to the vibration of the pin and diaphragm. Finally, the vibration of the diaphragm causes the sound radiation from the acoustic port. In addition to the above types of microspeakers and the balanced armature receiver, the piezoelectric speaker [8,9] has been developed and is known as a piezo bender due to its mode of operation. The mechanical motion of a piezoelectric speaker is created by applying a voltage to a piezoelectric material, and this motion is typically converted into sound using diaphragms. However, piezoelectric speakers have serious problems with their vibration material and cost.

Among these kinds of electroacoustic transducers, the microspeaker speaker is the most popular type in multimedia devices. The microspeaker is inserted into the microspeaker module and placed inside of a smartphon;, the relationship is depicted in Figure 1a. To ensure that people enjoy multimedia, it is necessary that the microspeaker module provides a good acoustic performance. Owing to the limitations of the inner space of portable electronic devices, the front chamber of a microspeaker module is usually designed as a side-firing type instead of a front-firing type, as shown in Figure 1b.

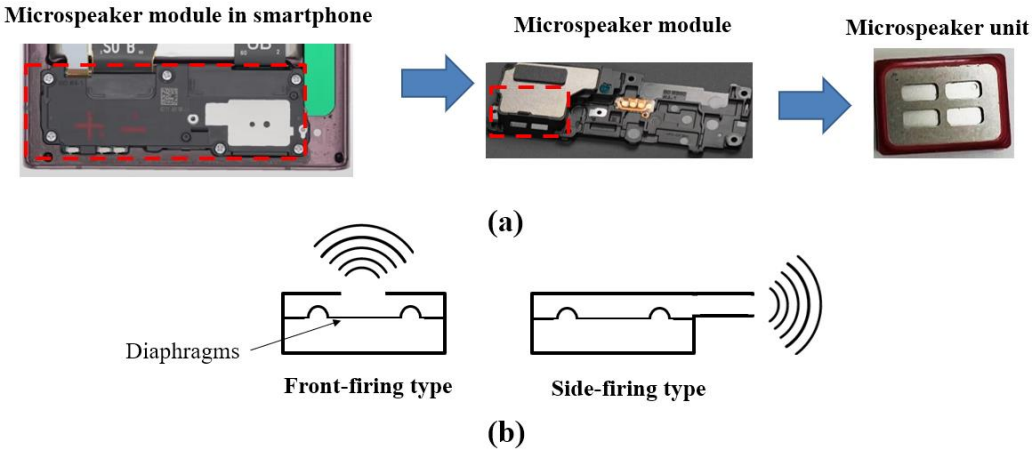


Figure 1. Microspeaker module: (**a**) microspeaker module and unit; (**b**) types of front chamber.

In previous studies, Xu et al. investigated the effect of an enclosure on a microspeaker. The back volume of the enclosure can be treated as the added stiffness of the mechanical system. However, the study did not discuss the effect of the front chamber on the sound pressure level [10]. Chang et al. discussed the acoustic performance of a microspeaker with different enclosure parameters. The main purpose of Chang's study was to identify the accuracy of the applied methodologies, but there was no discussion of the reason for the peaks around the middle and high frequencies in the side-firing front chamber [11].

In this study, the generating mechanisms of the mid-high frequency peaks of the microspeaker SPL are determined. The 3D electromagnetic–mechanical–acoustic (E-M-A) coupling method is used to obtain the whole sound pressure level of the microspeaker, while the resonance-calculated equations are only for predicting the mid-high peak frequencies. Microspeaker samples with different front chambers have been manufactured to verify the analysis results. The comparisons show good agreement between analysis peak frequencies and experimental peak frequencies. Thus, peak frequencies around mid-high frequency can be predicted by the proposed methods.

2. Analysis Methods

A microspeaker is an electroacoustic transducer that includes three physical domains. The first is an electromagnetic domain that consists of magnets, a voice coil, top plates, and a yoke. The permanent magnets are the source for the magnetic-field generation, resulting in a Lorentz force at the coil. The top plates and yoke gather the magnetic field from the permanent magnet, and it is concentrated at the coil.

The second is a mechanical domain that includes the voice coil, center diaphragm, side diaphragm, frame, protector, and suspension. The acoustic domain presents the air inside the front and back chambers. A 3D model of the microspeaker module is shown in Figure 2.

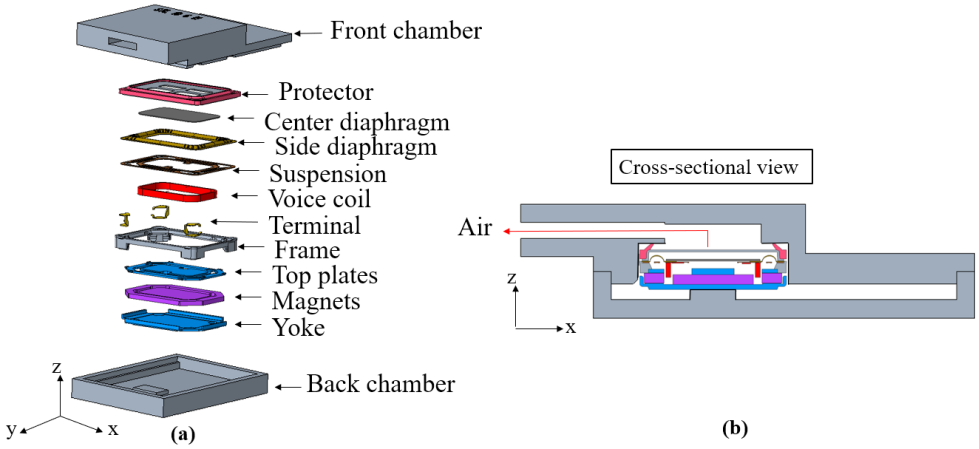


Figure 2. Structure of microspeaker module: (**a**) exploded view; (**b**) cross-sectional view.

2.1. Acoustic Modeling

There are three types of common acoustic modeling in a microspeaker module: a tube with two open ends [12], a closed cavity [13], and a Helmholtz resonator (HR) [14], as shown in Figure 3.

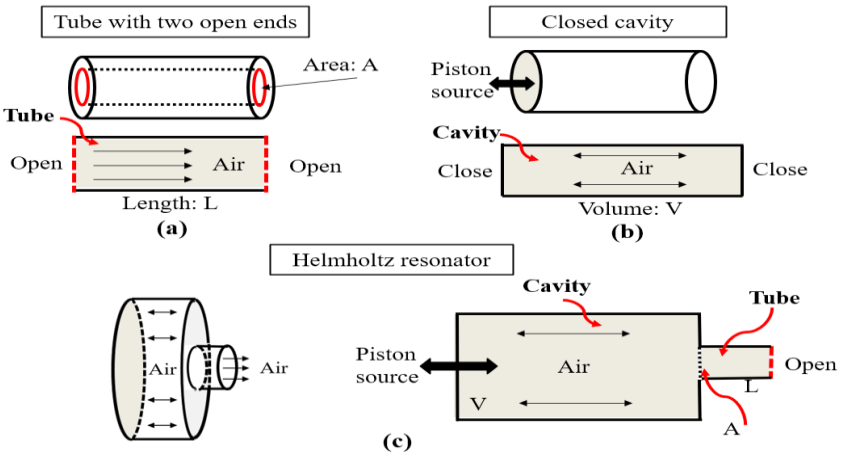


Figure 3. Acoustic modeling: (**a**) A tube with two open ends, (**b**) a closed cavity, and (**c**) a Helmholtz resonator.

A tube open at both ends with rigid walls behaves as an acoustic mass if it is sufficiently short, such that the air inside it moves without appreciable compression. The acoustic mass M_{ac} of the two open-end tubes is given by Equation (1).

$$M_{ac} = \frac{\rho L}{A} \left[\mathrm{kg/m^4}\right], \tag{1}$$

where ρ, L, and A denote the air density, tube length, and cross-sectional area, respectively. In the low-frequency limit, an applied external pressure compresses the enclosed air in the cavity, which then acts as a spring because of elasticity [15]. The acoustic spring constant of the closed cavity K_{ac} is given by Equation (2).

$$K_{ac} = \frac{\rho c^2}{V}\left[\mathrm{N/m^5}\right], \tag{2}$$

The direct analogy relationship between acoustic and mechanical analyses is shown in Equation (3).

$$M_{me} = M_{ac}A^2\ ,\ K_{me} = K_{ac}A^2, \tag{3}$$

where V, M_{me}, and K_{me} denote cavity volume, lumped mechanical mass, and lumped mechanical stiffness, respectively.

A Helmholtz resonator is type of resonator that consists of a cavity with a tube (narrow neck). A microspeaker can be thought of as a type of Helmholtz resonator because it has a cavity (the enclosure in which the speaker is mounted) and a tube (the front chamber of the speaker). When the speaker diaphragm moves back and forth, it causes pressure fluctuations in the air inside the enclosure, which can produce resonances in the cavity.

The geometrical correspondence between a microspeaker and a Helmholtz resonator is that both have a cavity and a tube and that both can produce resonances at certain frequencies. However, a microspeaker is more complex than a simple Helmholtz resonator because it also has a coil, magnets, and other mechanical parts that are responsible for converting electrical signals into mechanical motion. These parts also contribute to the resonant behavior of the speaker and affect its frequency response.

The Helmholtz resonator can be treated as a mechanical mass-spring system with a natural frequency f_{HR}, as shown in Equation (4). c is the speed of sound.

$$f_{HR} = \frac{1}{2\pi}\sqrt{\frac{K_{me}}{M_{me}}} = \frac{1}{2\pi}\sqrt{\frac{A^2\rho_0 c^2}{\rho_0 LAV}} = \frac{c}{2\pi}\sqrt{\frac{A}{LV}}, \tag{4}$$

In acoustics [16], end correction [17,18] is a short distance applied or added to the actual length of a resonance tube to calculate the precise resonant frequency.

Hydraulic diameter [19] is a commonly used term for handling flow in noncircular tubes and channels. Using this term, one can calculate flow for a noncircular tube in the same way as for a circular tube. If the cross section has a rectangular shape with width b and height a, the hydraulic diameter is given by Equation (5).

$$D_h = \frac{2ab}{a+b}\ ,\ b \gg a, \tag{5}$$

The Helmholtz resonator considering an end correction (HREC) is given by Equation (6):

$$f_{HREC} = \frac{c}{2\pi}\sqrt{\frac{A}{(L+0.85D_h)V}}, \tag{6}$$

The resonance frequencies of the two open-end tubes considering an end correction (TEC) are shown in Equation (7).

$$f_{TEC} = \frac{c}{2(L+0.8D_h)}, \tag{7}$$

The air volume of the cavity is 156.34 mm^3. The peak frequencies calculated using Equations (6) and (7) are defined as method #1. The 3D E–M–A coupling method [20] is used to obtain the SPL curve, which is regarded as method #2.

2.2. Back Chamber Effect

A microspeaker can be assumed as an element of a mass, a spring, and a damping (MCK) system with a forced vibration. It is inserted into a back chamber to prevent the leakage of sound having an opposite phase from the backside of the diaphragm. Owing to space limitation in smartphones, the back volume in the speaker box is always limited. The back volume is a small, closed air volume under the diaphragms that includes the center diaphragm (CDP) and the side diaphragm (SDP). The back volume adds additional stiffness to the mechanical system of the microspeaker (unit stiffness), resulting in an increased fundamental resonance frequency.

The fundamental resonance frequency is determined by the moving mass and the total stiffness of the mechanical system. The cross-sectional view of the microspeaker unit is shown in Figure 3a. The material of SDP is an elastomer compound, and it has the lowest Young's modulus. The CDP is a flat plate made by aluminum compound to keep the coil vibrating uniformly. The unit stiffness is controlled by the material and structure of SDP; the vibration mode of diaphragms and voice coil is shown in Figure 4; the other parts have been hidden.

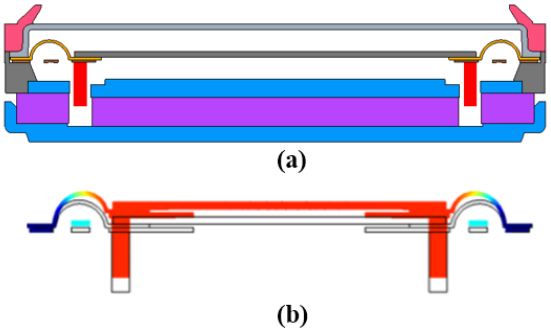


Figure 4. Vibration mode: (**a**) cross-section view of microspeaker unit and (**b**) the vibration mode of diaphragms and voice coil.

The mechanical parts work together to convert electrical signals into mechanical motion, which creates sound waves in the surrounding air. The stiffness and the mass of moving parts affect the speed at which the diaphragms can move and the mount of force it can generate. This, in turn, affects the frequency response and the volume of the sound produced by the microspeaker. A heavier coil or more flexible diaphragm will result in a lower resonance frequency, which means the microspeaker will be less capable of producing high-frequency SPL. A lighter coil or a more rigid diaphragm will result in a higher resonance frequency, which means the microspeaker will be more capable of producing high-frequency SPL.

The microspeaker can also ideally be represented as a rigid piston at low frequencies because the movement of the diaphragm is similar to the movement of a piston in an engine, as shown in Figure 5. The added stiffness [21] can be calculated by Equation (8). The relationship between total stiffness, unit stiffness, and added stiffness is shown in Equation (9). The unit stiffness is only determined by the mechanical structure and material of the diaphragms; thus, it can be obtained by mechanical analysis. The total stiffness is the sum of unit stiffness and added stiffness, which determined the fundamental resonance of microspeaker. The fundamental resonance frequency can be expressed as Equation (10).

$$K_{added} = \frac{\rho_0 c^2 {S_d}^2}{V_{back}}, \tag{8}$$

$$K_{Total} = K_{Unit} + K_{added}, \tag{9}$$

$$f_0 = \frac{1}{2\pi}\sqrt{\frac{K_{Total}}{M}}, \tag{10}$$

where ρ_0 is a density of air. S_d is the effective radiation area [22]. V_{back} is the back volume. f_0 is the fundamental resonance frequency, which the first peak shows in the SPL curve around 1 kHz. M is the moving mass of the mechanical system that mainly comes from the voice coil and center diaphragm.

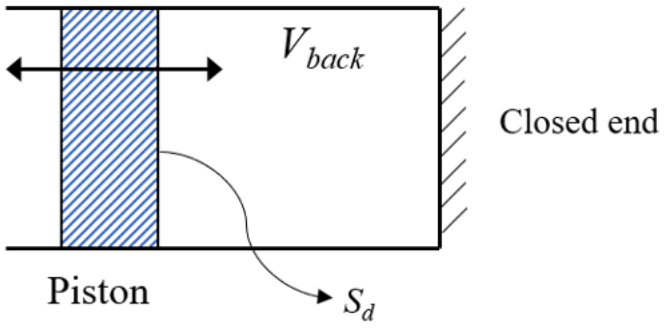


Figure 5. Piston source model.

2.3. E–M–A Coupling Model

The E–M–A coupling method of the microspeaker uses the coupled equations of the voltage, mechanical vibration, and acoustic wave equations, which are shown in Equations (11)–(13), respectively.

$$V_e = IR_e + L_e\frac{dI}{dt} + Bl\dot{z}, \tag{11}$$

where V_e, I, R_e, Bl, and $\dot{z}$ are the input voltage, electrical current, direct current resistance of the voice coil, inductance, force factor, and mechanical velocity, respectively.

$$[M]\{\ddot{z}\} + [R]\{\dot{z}\} + [K]\{z\} = \{F_L\}+\{F_P\}, \tag{12}$$

where $[M]$, $\{\ddot{z}\}$, $[R]$, $\{\dot{z}\}$, $[K]$, $\{z\}$, $\{F_L\}$, and $\{F_P\}$ are the mass, acceleration, damping, velocity, stiffness, displacement, Lorentz force, and pressure force vectors, respectively.

$$\nabla^2 P + k^2 P = 0, \tag{13}$$

where ∇^2, P, and k are the Laplace operator, acoustic pressure, and wave number, respectively.

Equations (14)–(17) indicate the coupled relationships between the electromagnetic, mechanical, and acoustic domains.

$$V_{Backemf} = Bl\dot{z}, \tag{14}$$

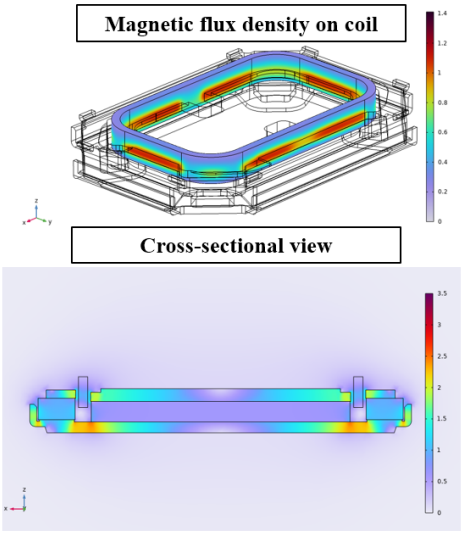
$$F_L = BlI, \tag{15}$$

$$F_P = S_d P, \tag{16}$$

$$U = S_d\dot{z}, \tag{17}$$

where $V_{Backemf}$ and U represent the back electromotive force and volume velocity, respectively.

The coil information, magnetic flux density on the coil, the flux density distribution in cross-section, and the force factor of the microspeaker are shown in Figure 6. The material of the magnets is neodymium with magnet grade N52H. The voice coil is the Daikoku high-tension wire (DHT), which can provide a high tensile strength. SDP is an elastomer compound, while the CDP is an aluminum compound. The top plates and yoke are made of steel plate cold commercial (SPCC).The material of frame and protector are polycarbonate and stainless steel (SUS 301), respectively. The front and back chamber are made by a 3D printer with printing material Nylon 11. The mechanical material properties are shown in Table 1.



Magnetic flux density on coil	
DCR [ohm]	6.0
Coil diameter [mm]	0.077
Coil turn	51.5
Coil length [mm]	1535.1
Flux density [T]	0.577
Force factor [N/A]	0.887

Figure 6. Electromagnetic analysis results.

Table 1. Mechanical material properties.

Part	Material	Density [kg/m^3]	Young's Modulus [GPa]	Poisson's Ratio
Magnet	N52H	7790.0	41.4	0.29
Voice coil	DHT	5320.0	110	0.35
Suspension	Polyimide Film	2110.0	2.50	0.34
SDP	Elastomer Compound	1230.0	0.13	0.40
CDP	Aluminum Compound	856.1	69.3	0.28
Yoke	SPCC	7308.0	190	0.29
Frame	Polycarbonate	1165.0	2.4	0.37
Protector	SUS 301 1/4H	7551.0	193	0.28
Chambers	Nylon 11	1040.0	0.335	0.32

E–M–A coupling analysis is performed to derive the SPL of a microspeaker. For the accurate analysis of complex acoustic structures, FEM is used instead of the lumped parameter method (LPM) [23]. The boundary condition should be well defined, simulating the real experimental environment, where it is in an anechoic chamber. A spherical air region is formed, and the boundary condition of outward spherical wave radiation is applied at the exterior surface. The special wave radiation boundary condition can provide minimal reflections to the acoustic wave. The SPL comparison between analysis results and experiment results shows that the spherical wave radiation boundary condition is good enough for the acoustic analysis of the microspeaker. The E–M–A coupling model is illustrated in Figure 7.

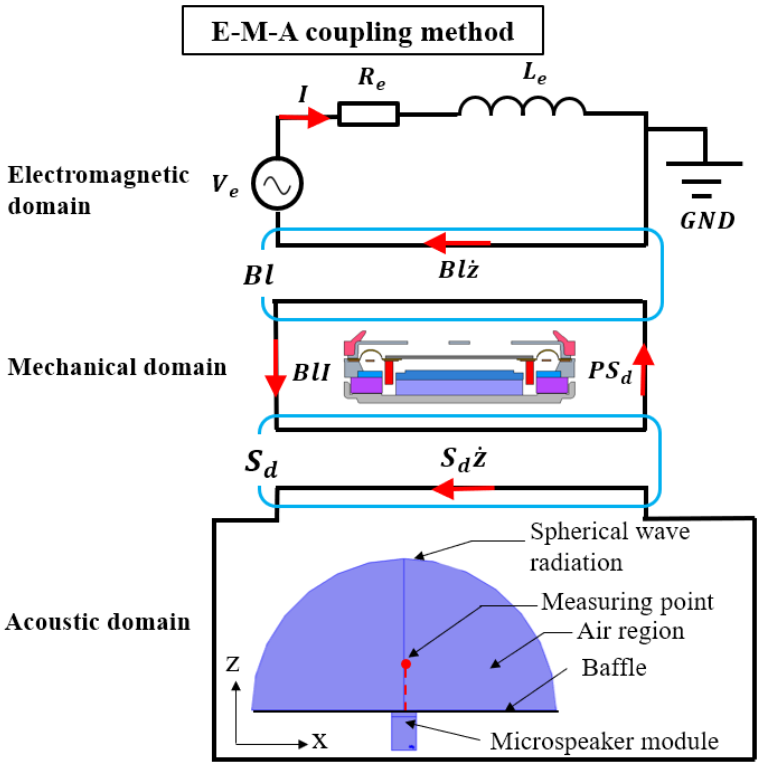


Figure 7. Electromagnetic–mechanical–acoustic coupling model.

3. Experimental and Verification

The Type 1 module consists of a front chamber, microspeaker unit, and back chamber, as shown in Figure 8a. A B&K measurement system is used to obtain the SPL results, which included a monitor, computer host, a pulse multi-analyzer (B & K 3560C), a power amplifier (B & K 2718), a microphone (B & K 4191), and baffles, as shown in Figure 8b. B & K is the shorthand for the company's name (Brüel & Kjær, Nærum, Denmark). The microphone is placed inside the anechoic chamber, and other devices are placed outside the chamber. The sound signal recorded by the microphone is transformed into SPL in frequency domain using fast Fourier-transform (FFT).

The microspeaker module is fixed to the small baffle and inserted on the big baffle using two clamps. The baffles prevent sound coming from the backside of the baffle from affecting the SPL measurement. The microphone is placed at a distance of 10 cm from the central axis of the microspeaker module. The input voltage is 3.1 Vrms with sinusoidal signal sweeping from 100 Hz to 20 kHz. The octave band is 1/12 oct.

The SPL comparison of type 1 module between the analysis and experimental results is shown in Figure 8c, which shows a good match.

A comparison of the peak frequencies between the analysis and experimental results for the type 1 module is shown in Table 2. The peak frequencies predicted by method #1 and method #2 are in good agreement with the experimental results.

Table 2. Peak frequencies comparison of type 1 module.

Type	f_{HREC} (Method #1/Method #2/Expt.)	f_{TEC} (Method #1/Method #2/Expt.)
Type 1	3099/3150/3000	14,929/15,000/15,000

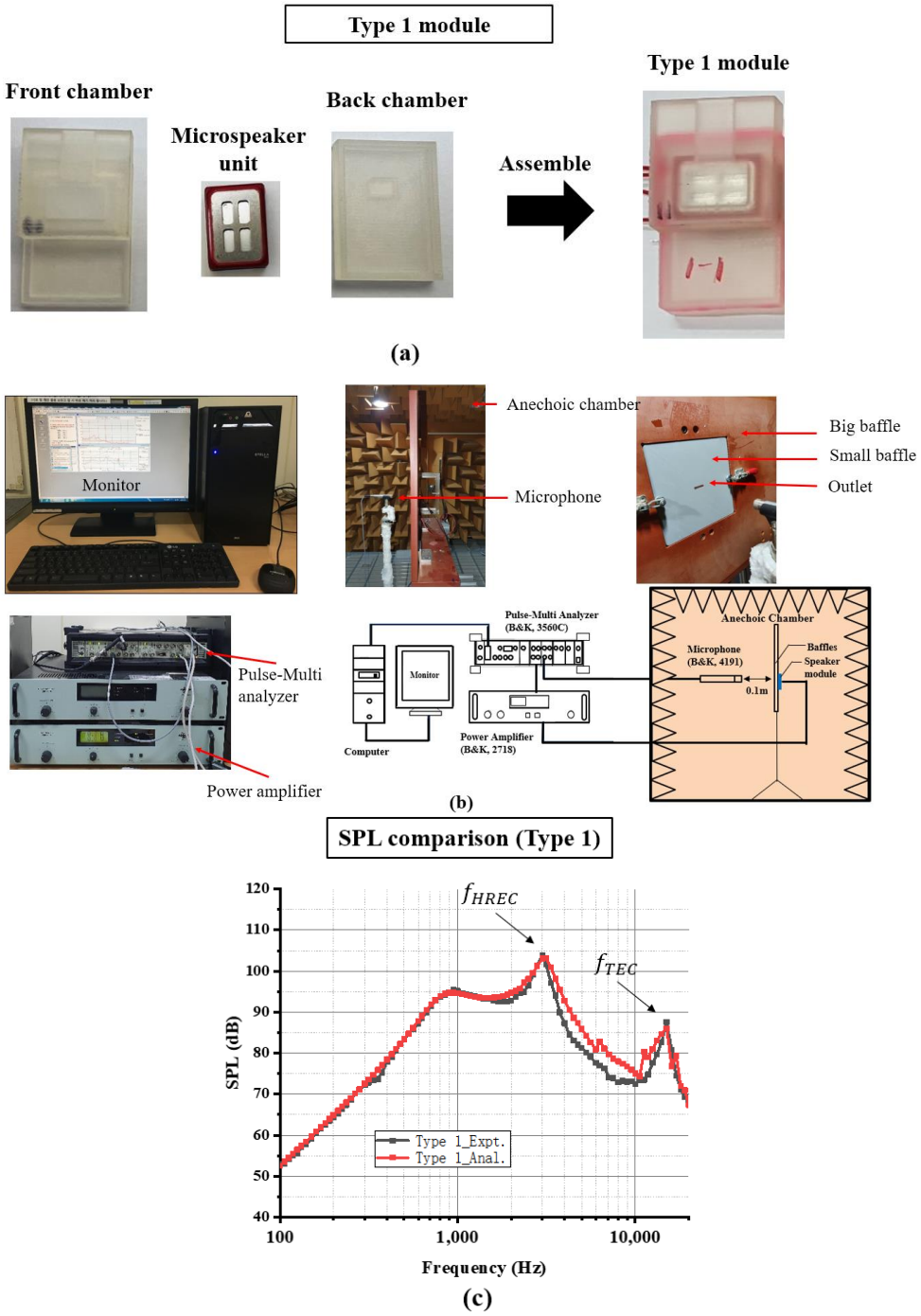


Figure 8. Experimental setup and results: (**a**) microspeaker module samples, (**b**) the schematic of B&K setup, and (**c**) SPL comparison (Type 1).

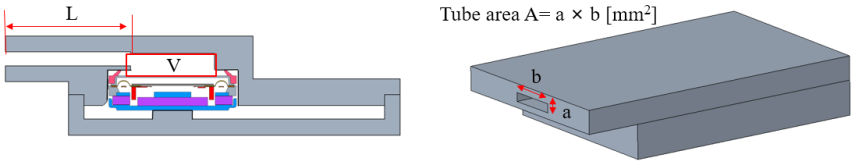
4. Side-Firing Front Chamber Designs

Type 1 module is regarded as the reference module, and six new modules are designed to determine the influence of the tube parameters on the peak frequencies (f_{HREC} and f_{TEC}). The air volume in front of the diaphragm of the microspeaker is set as the fixed value.

The tube shape is designed as rectangular in order to control the design parameters easily. The design parameters are selected as tube length, tube width, and tube height. The tube area is controlled by the tube width and tube height directly.

The design range of tube length is from 8.0 mm to 12.0 mm, step 2.0 mm. The tube width are set as 4.0 mm, 6.0 mm, and 8.0 mm to control the tube area from type 1 to type

5. The tube height is set as a constant value of 1.10 mm with the consideration of the real situation in smartphones. In type 6 and type 7, the tube width and tube height have been changed to remain the same tube area as 6.60 mm^2. A comparison of modules with different side-firing front chambers is shown in Figure 9.



Type of module	Tube length L	Tube width b	Tube height a	Tube area A
Type 1	10.0	6.0	1.10	6.60
Type 2	8.0	6.0	1.10	6.60
Type 3	12.0	6.0	1.10	6.60
Type 4	10.0	4.0	1.10	4.40
Type 5	10.0	8.0	1.10	8.80
Type 6	10.0	8.25	0.80	6.60
Type 7	10.0	5.08	1.30	6.60

Figure 9. Different tube designs.

Type 1, Type 2, and Type 3 are in the first group that is used to investigate the tube length effect on mid-high frequency peaks.

Type 1, Type 4, and Type 5 are in the second group with different tube widths to investigate the tube width (tube area) effect on mid-high frequency peaks.

Furthermore, the last group includes Type 1, Type 6, and Type 7, maintaining the same tube length and tube area but different combination of tube width and tube height.

5. Results and Discussions

The side-firing front chamber designs are manufactured by using a 3D printer, as shown in Figure 10a. Type 1, type 2, and type 3 have the same tube width and tube height but different tube lengths. Type 1, type 4, and type 5 have the same tube length and tube height but different tube widths, which causes the different tube areas, while type 1, type 6, and type 7 keep the same tube length and the same tube area controlled by the tube width and tube height. The microspeaker unit and different side-firing front chambers are assembled together, as shown in Figure 10b.

An experimental SPL comparison between the different side-firing front chamber designs is shown in Figure 11. In the first group, the type 2 has biggest f_{HREC} and f_{TEC}, and the frequency of mid-high frequency peaks sorted from big to small is type 2, type 1, type 3, as shown in Figure 11a. In the second group, all types' f_{TEC} are the same, while the f_{HREC} are different, and the frequency of mid frequency peaks sort from big to small is type 5, type 1, type 4, as shown in Figure 11b. In the last group, all types have the same mid-high frequency peaks even though they have different tube widths and tube lengths, as shown in Figure 11c. A mid-high peak frequencies comparison between the different prediction methods is presented in Table 3.

According to the above results, the following conclusions are obtained:

1. The longer tube length (the same tube area), the lower f_{HREC} and the lower f_{TEC}.
2. A wider tube width (the same tube length) causes a higher f_{HREC} owing to the larger tube area. The tube width has a slight influence on f_{TEC} when the end correction is considered.
3. With different tube widths and tube heights (the same tube length), the f_{HREC} can be similar when the tube area remains the same.

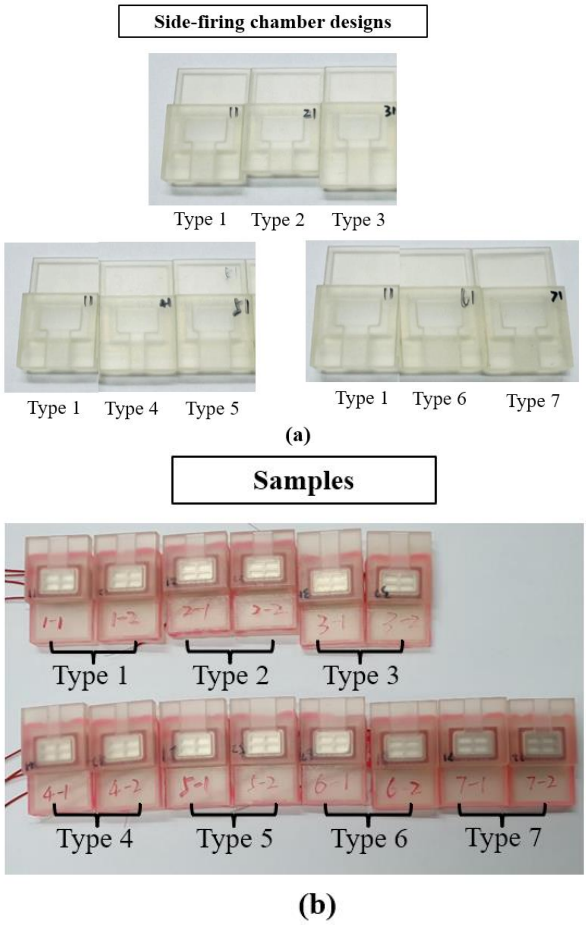


Figure 10. Different side-firing front chamber samples: (**a**) The side-firing chamber; (**b**) The different samples.

Table 3. Peak frequencies comparison (All types).

Type	f_{HREC} (Method #1/Method #2/Expt.)	f_{TEC} (Method #1/Method #2/Expt.)
Type 1	3099/3150/3000	14,929/15,000/15,000
Type 2	3408/3350/3350	18,076/17,000/17,000
Type 3	2862/2800/2800	12,715/13,200/13,200
Type 4	2543/2650/2650	15,069/15,000/15,000
Type 5	3569/3350/3350	14,852/15,000/15,000
Type 6	3146/3150/3150	15,357/15,000/15,000
Type 7	3075/3000/3000	14,713/14,000/15,000

The mid-high peak frequencies can be calculated according to the dimensions of the tube and cavity using method #1. However, it cannot predict the SPL result, whereas method #2 can predict the SPL results and mid-high peak frequencies well. The SPL comparisons between the experimental results and the E–M–A coupling analysis results are shown in Figure 12.

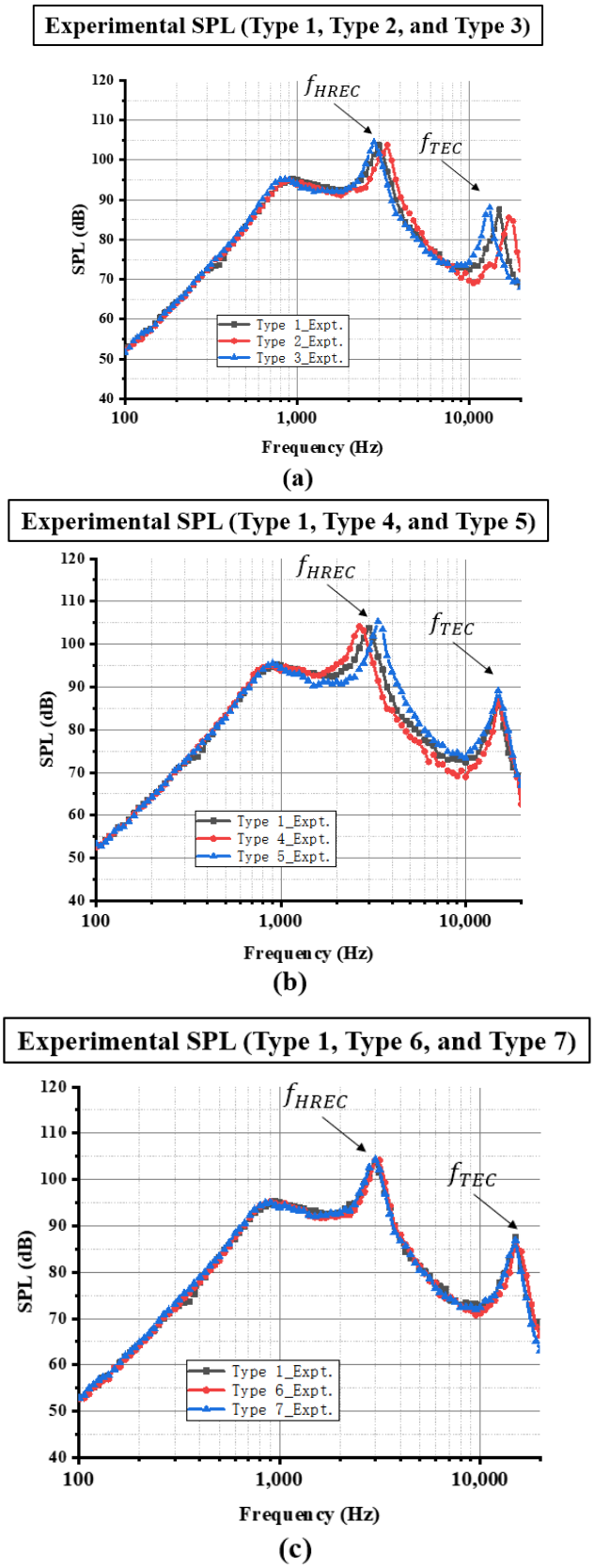


Figure 11. Experimental SPL comparison: (**a**) type 1, type 2, and type 3; (**b**) type 1, type 4, and type 5; (**c**) type 1, type 5, and type 6.

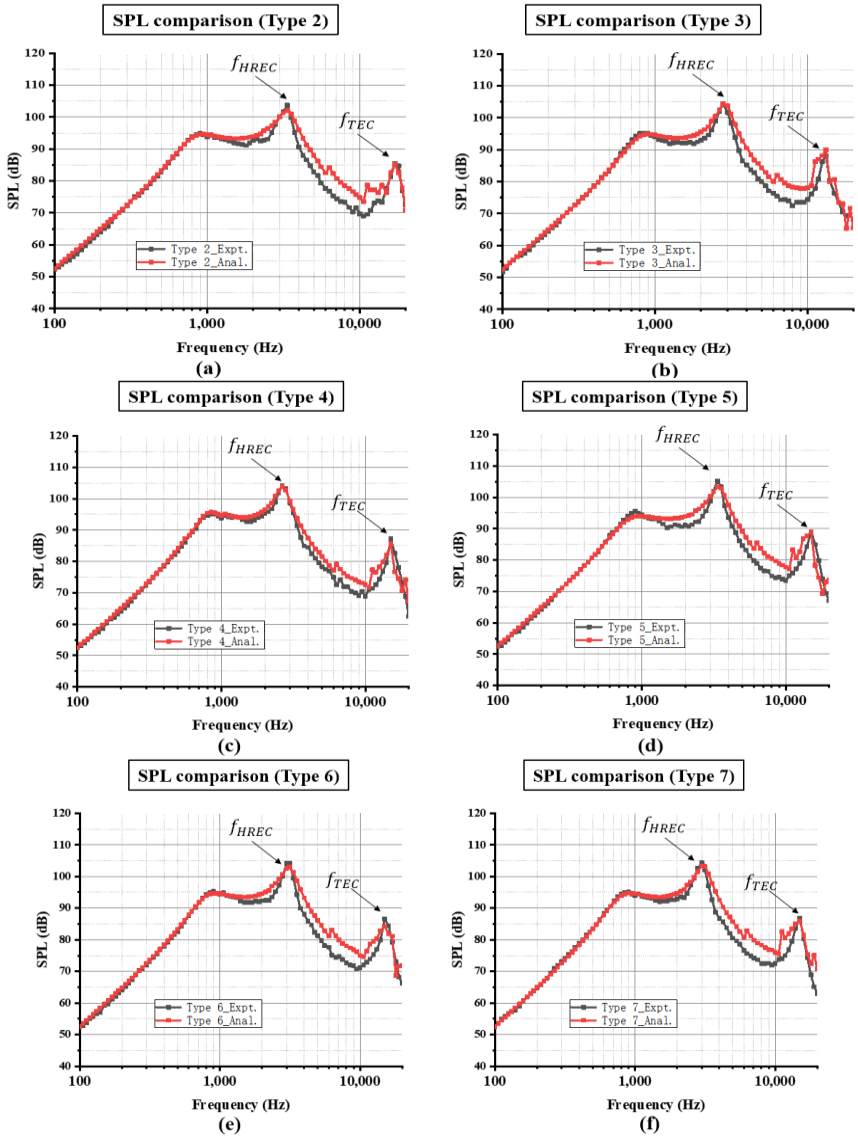


Figure 12. SPL Comparison between experimental and analysis results. (**a**) Type 2, (**b**) Type 3, (**c**) Type 4, (**d**) Type 5, (**e**) Type 6, (**f**) Type 7.

The microspeaker has a frequency response curve with certain frequencies at which the sound pressure output is particularly strong. These frequencies may be perceived as being more "loud" or "intense" by the listener, and they may also be associated with specific types of sounds.

The advantage of mid-high frequency peaks to the user may depend on the specific frequencies and intensities involved, as well as the listener's individual auditory perception and preferences. For example, if the peaks occur at frequencies that correspond to certain musical notes or other sounds that are important to the listener, then these peaks may be perceived as enhancing the overall quality or clarity of the audio output. On the other hand, if the peaks are too pronounced or occur at frequencies that are unpleasant or jarring to the listener, they may be perceived as a disadvantage.

It is important to note that the perception of sound is subjective, and what is perceived as an advantage or disadvantage may vary from person to person. Additionally, the SPL curve of a microspeaker may be affected by a number of factors, including the design and construction of the speaker, the characteristics of the enclosure or cabinet in which it is placed, and the audio signal being applied to it.

6. Conclusions

This study investigates the cause of mid-high frequency peaks on a microspeaker SPL curve. The mid-frequency peak is caused by a Helmholtz resonator, which is a type of air-filled chamber that is attached to the speaker. The length, width, and height of the cavity can all affect the resonant frequency of the Helmholtz resonator, which in turn can affect the overall frequency response of the speaker. The high-frequency peak is caused by the tube resonator, which is only relative to the tube length. The proposed methods (methods #1 and #2) are verified experimentally. The SPL and mid-high peak frequencies comparisons show good agreement between the analysis and experimental results, which indicates that the spherical wave radiation boundary condition is good enough for the E–M–A coupling analysis of the microspeaker. The mid-high frequency peaks on the SPL curve of a microspeaker can affect the auditory perception of listeners in different ways, as perceptions of sound are subjective. This study provides insight into the acoustic performance of microspeakers in the mid-high frequency range and can serve as a design tool for side-firing front chambers. By understanding the factors that contribute to these peaks and how they may be influenced, designers and engineers can create microspeakers that are better suited to the needs and preferences of their intended users.

Author Contributions: Conceptualization, Z.-X.J. and S.-M.H.; methodology, Z.-X.J. and D.-P.X.; software, Z.-X.J.; validation, Z.-X.J. and D.-P.X.; formal analysis, Z.-X.J. and J.-H.P.; investigation, Z.-X.J. and J.-H.P.; resources, Z.-X.J.; data curation, Z.-X.J. and J.-H.P.; writing—original draft preparation, Z.-X.J.; writing—review and editing, Z.-X.J. and J.-H.P.; visualization, Z.-X.J.; supervision, D.-P.X. and S.-M.H.; project administration, S.-M.H.; funding acquisition, S.-M.H. All authors have read and agreed to the published version of the manuscript.

Funding: This research is funded by a 2-Year Research Grant of Pusan National University.

Institutional Review Board Statement: Not applicable.

Informed Consent Statement: Not applicable.

Data Availability Statement: Not applicable.

Conflicts of Interest: The authors declare no conflict of interest.

References

1. Jiang, Z.X.; Park, J.H.; Xu, D.P.; Hwang, S.M. Analysis and Prediction of Mid-high Peak Frequencies for Microspeaker with Side-firing Front Chamber. In Proceedings of the IEEE 20th Biennial Conference on Electromagnetic Field Computation (CEFC), Denver, CO, USA, 24–26 October 2022; pp. 1–2.
2. Hwang, S.M.; Hwang, G.Y.; Kwon, J.H.; Lee, H.J.; Kang, B.S. Performance comparison between circular and elliptical type microspeakers for cellular phones. *IEEE Trans. Magn.* **2003**, *39*, 3256–3258. [CrossRef]
3. Hwang, S.M.; Lee, H.J.; Hong, K.S.; Kang, B.S.; Hwang, G.Y. New development of combined permanent-magnet type microspeakers used for cellular phones. *IEEE Trans. Magn.* **2005**, *41*, 2000–2003. [CrossRef]
4. Kwon, J.H.; Hwang, S.M.; Kim, K.S. Development of slim rectangular microspeaker used for minimultimedia phones. *IEEE Trans. Magn.* **2007**, *43*, 2704–2706. [CrossRef]
5. Lee, C.M.; Kwon, J.H.; Hwang, G.Y.; Hwang, S.M. Development of a new magnetic circuit for slim microspeakers. *J. Appl. Phys.* **2009**, *105*, 07E710. [CrossRef]
6. Xu, D.P.; Lu, H.W.; Jiang, Y.W.; Kim, H.K.; Kwon, J.H.; Hwang, S.M. Analysis of sound pressure level of a balanced armature receiver considering coupling effects. *IEEE Access* **2017**, *5*, 8930–8939. [CrossRef]
7. Jiang, Y.W.; Xu, D.P.; Hwang, S.M. Electromagnetic-mechanical analysis of a balanced armature receiver by considering the nonlinear parameters as a function of displacement and current. *IEEE Trans. Magn.* **2018**, *54*, 1–4.
8. Kim, H.J.; Yang, W.S.; No, K. Improvement of low-frequency characteristics of piezoelectric speakers based on acoustic diaphragms. *IEEE Trans. Ultrason. Ferroelectr. Freq. Control.* **2012**, *59*, 2027–2035. [CrossRef] [PubMed]
9. Chiang, H.Y.; Huang, Y.H. Resonance mode and sound pressure produced by circular diaphragms of electrostatic and piezoelectric speakers. *Appl. Acoust.* **2018**, *129*, 365–378. [CrossRef]
10. Xu, D.P.; Jiang, Y.W.; Kwon, J.H.; Hwang, S.M. Analysis of the effects of electromagnetic circuit variables on sound pressure level and total harmonic distortion in a balanced armature receiver. *IEEE Trans. Magn.* **2017**, *53*, 1–4. [CrossRef]
11. Chang, J.R.; Wang, C.N. Acoustical analysis of enclosure design parameters for microspeaker system. *J. Mech.* **2019**, *35*, 1–12. [CrossRef]

12. Kinsler, L.E.; Frey, A.R.; Coppens, A.B.; Sanders, J.V. *Fundamentals of Acoustics*, 4th ed.; John Wiley & Sons: Hoboken, NJ, USA, 2000.
13. Kleiner, M. *Electroacoustics*; CRC Press: Boca Raton, FL, USA, 2013.
14. Breazeale, M.A.; Leroy, O. *Physical Acoustics: Fundamentals and Applications*; Springer Science & Business Media: Berlin/Heidelberg, Germany, 2012.
15. Beranek, L.L.; Mellow, T. *Acoustics: Sound Fields and Transducers*, 2nd ed.; Academic Press: Cambridge, MA, USA, 2012.
16. Raichel, D.R. *The Science and Applications of Acoustics*, 2nd ed.; Springer: Berlin/Heidelberg, Germany, 2006; pp. 145–149.
17. Ruiz, M.J. Boomwhackers and End-Pipe Corrections. Available online: http://www.mjtruiz.com/publications/2014_boomwhackers.pdf (accessed on 20 February 2014).
18. End Correction at a Flue Pipe Mouth. Available online: http://www.fonema.se/mouthcorr/mouthcorr.htm (accessed on 30 September 2006).
19. Chanson, H. *Environmental Hydraulics for Open Channel Flows*; Elsevier: Amsterdam, The Netherlands, 2004.
20. Jiang, Z.X.; Park, K.H.; Hwang, S.M. Design and Analysis of Watch Speaker to Enhance Waterproof Performance by Using Liquid Silicone Rubber Side Diaphragm. *Sens. Actuators A Phys.* **2022**, *338*, 11345. [CrossRef]
21. Sun, P.; Xu, D.P.; Hwang, S.M. Design of microspeaker module considering added stiffness. *J. Mech. Sci. Technol.* **2014**, *28*, 1623–1628. [CrossRef]
22. Klippel, W.; Schlechter, J. Dynamical measurement of the effective radiation area SD. In *Audio Engineering Society Convention 128*; Audio Engineering Society: New York, NY, USA, 2010.
23. Bai, M.R.; Chen, R.L.; Wang, C.J. Electroacoustic analysis of an electret loudspeaker using combined finite-element and lumped-parameter models. *J. Acoust. Soc. Am.* **2009**, *125*, 3632–3640. [CrossRef]

Disclaimer/Publisher's Note: The statements, opinions and data contained in all publications are solely those of the individual author(s) and contributor(s) and not of MDPI and/or the editor(s). MDPI and/or the editor(s) disclaim responsibility for any injury to people or property resulting from any ideas, methods, instructions or products referred to in the content.